Anharmonic Coupling in Molecular Dynamics Simulations of Ligand Vibrational Relaxation in Bound Carbonmonoxy Myoglobin

Michael Devereux and Markus Meuwly*

Department of Chemistry, University of Basel, Klingelbergstrasse 80, 4056 Basel, Switzerland

Received: April 23, 2009; Revised Manuscript Received: July 7, 2009

Vibrational relaxation of CO bound to myoglobin (MbCO) following photoexcitation is investigated using nonequilibrium molecular dynamics (MD) simulations. It is found that harmonic potential energy functions for bond vibrations are not suited to simultaneously and accurately describe vibrational de-excitation and the vibrational spectroscopy of the bound ligand. Only when anharmonic (e.g. Morse) potentials are introduced for both the C−O and the adjacent Fe−C_{CO} bonds to allow anharmonic coupling, rapid (tens of ps) relaxation of the vibrationally excited CO is possible. To capture both relaxation and vibrational spectroscopy, the parameters of the potential energy functions are fitted by an interactive, nonlinear least-squares procedure using averages over multiple MD trajectories. The sensitivity of cooling rate to the difference in vibrational frequency between coupled modes is demonstrated. Potential cooling mechanisms are suggested, based on the sensitivity of the CO relaxation rate to changes in the force field parameters of local degrees of freedom. Accounting for quantum correction leads to relaxation rates around 20 ps, in good agreement with experiment. Finally, the importance of electronic effects is explored by fitting a 2D potential energy surface to *ab initio* data to describe the strengthening and weakening of the CO bond as a function of Fe−C_{CO} bond length, and vice versa.

I. Introduction

Vibrational spectroscopy provides a powerful and accurate means to probe the structure and dynamics of a molecular system. Many forms of photon absorption and emission spectroscopy are used in almost every area of chemistry, and very informative vibrational spectra can be obtained for systems ranging from simple diatomic molecules to macromolecules such as proteins. Vibrational data are therefore a useful and reliable reference to parametrize atomistic force fields for molecular dynamics simulations. An accurate representation of vibrations may be particularly important when implementing reactive dynamics, where bond breakage leads to release of energy and local heating effects. Modeling vibrational coupling may also be important in large proteins when describing energy transfer pathways which are believed to coincide with propagation pathways for conformational change in protein allostery.[1,2] For example, it was found that energy transfer pathways in the PSD-95 protein after local heating were closely linked to the hypothesized allosteric signal pathway identified using evolutionary data of conserved residues.[1]

Substantial progress has been made in observing and modeling bond relaxation after photoexcitation in large biomolecular, and smaller model systems.[3−9] Various approaches exist, perhaps the most intuitive of which use nonequilibrium MD simulations[3] to explicitly excite the bond(s) of interest and measure relaxation time. By averaging over a number of nonequilibrium trajectories, a cooling time T_1 is obtained according to[10,11]

$$\frac{\overline{E_v(t)} - \overline{E_v(\infty)}}{\overline{E_v(0)} - \overline{E_v(\infty)}} = \exp(-t/T_1) \qquad (1)$$

Here, $E_v(t)$ is the vibrational energy at time t, T_1 is the vibrational relaxation time, and the overbar represents an average over nonequilibrium trajectories. $\overline{E_v(\infty)}$ can be assumed to take the thermal value[6] k_BT (0.60 kcal/mol at 300 K), while $E_v(0)$ is the initial vibrational energy of the excited bond at $t = 0$.

An alternative approach calculates T_1 from equilibrium MD simulations[6] using the autocorrelation function of the fluctuating scalar force along a given bond. If the vibrational frequency of the bond is high, the bond vibration can be treated as approximately static and constrained to its equilibrium length in simulations, only measuring fluctuation in the forces acting along the constrained bond. Results obtained using this equilibrium approach were found to be very similar to those obtained using nonequilibrium simulations with fits to eq 1.[3]

A third approach uses normal modes[12,13] to calculate the forces applied to a given "system mode". T_1 can then be either calculated directly or indirectly by first obtaining the "quantum correction factor" (QCF) to link the classical mechanical value of T_1 to its more accurate quantum mechanical value.[14]

Here, the first approach based on nonequilibrium simulations to explicitly excite the CO bond and measure cooling times is used, previously found to yield meaningful results for CN relaxation in MbCN.[9] Because relaxation involves coupling between different—mainly vibrational—degrees of freedom, calculated relaxation times depend on the details with which interactions in the force field are described. Most commonly used force fields are based on harmonic functions for bonded interactions (bonds r and valence angles θ) and periodic functions for torsions ϕ to describe the total energy as a function of molecular structure. For example, the CHARMM force field is based on the following parametrization:[15]

$$E = \sum_{\text{bonds}} k_b(r - r_0)^2 + \sum_{\text{angles}} k_\theta(\theta - \theta_0)^2 + \sum_{\text{torsions}} k_\phi[1 + \cos(n\phi - \delta)] + \sum_{\text{impropers}} k_\psi(\psi - \psi_0)^2 + \sum_{\text{Urey−Bradley}} k_{UB}(r_{1,3} - r_{1,3,0})^2 + \sum_{\text{VDW}} \varepsilon_{ij}\left[\left(\frac{R_{\min,ij}}{r_{ij}}\right)^{12} - 2\left(\frac{R_{\min,ij}}{r_{ij}}\right)^{6}\right] + \sum_{\text{electrostatics}} \frac{q_iq_j}{r_{ij}} \qquad (2)$$

10.1021/jp903741v CCC: $40.75 © 2009 American Chemical Society
Published on Web 09/02/2009

where k_b, k_θ, k_ϕ, k_ψ, and k_{UB} are the bond, bond-angle, torsional, improper dihedral, and Urey−Bradley force constants, respectively. The coordinates involved are r, θ, ϕ, ψ, and $r_{1,3}$ for the bond length, bond angle, dihedral angle, improper dihedral angle, and Urey−Bradley 1,3 distance, respectively, and the subscript "0" denotes the equilibrium value for each coordinate. Nonbonded Lennard-Jones parameters include the "well depth", ε, and the interaction distance at the energy minimum, R_{min}. Atomic charges used to calculate electrostatic interactions between atoms i and j are denoted q, and r_{ij} is their distance.

Both the bonded and angular bending terms in this model are harmonic. The energy profiles of chemical bonds in real molecules are, however, anharmonic in nature: the restoring force of a bond is not strictly proportional to r but rather asymptotically approaches zero as the bond is stretched and broken. One consequence of using harmonic bonded terms is that for a given total energy the density of states obtained is lower than that obtained using anharmonic terms, which reduces the efficiency of vibrational coupling between adjacent vibrational modes. Harmonic coupling becomes especially inefficient where the difference in vibrational frequency between the coupled modes is large.[8]

The charge model used to describe the nonbonded interactions of the atoms of an excited normal mode has also been found to affect relaxation time in certain systems. An excited CH_3Cl molecule in a polar solvent was found to have T_1 values of 100, 4.5, and 1.4 ps when no charge, normal charges, and doubled charges were used in the simulations, respectively.[3] In a further study,[16] vibrational energy transfer between HF molecules and vibrational modes of nearby solvent water molecules was also affected by the charge model used. Switching from point charges to a point dipole model significantly reduced the efficiency of vibrational coupling to nonbonded vibrational modes. Experimental Raman data also suggest significant nonbonded coupling interactions exist between metal-octaethylporphyrins and organic solvent modes.[17] Additional studies involving diatomic molecules in liquids, however, suggest that electrostatic forces play a minor role in vibrational relaxation in many systems.[18] The role of electrostatic interactions in CO relaxation in Mb will therefore be investigated.

Finally and of particular interest for bound MbCO, is the role of back-bonding interactions between the CO ligand and the heme-Fe center of the Mb active site. Previously, strong negative correlation between the CO and Fe−C_{CO} bond lengths has been found, as back-donation from the Fe(II) d_π orbitals to the CO π^* orbitals strengthens the Fe−C_{CO} bond, at the expense of the CO bond.[19] It is unclear what effect this correlation will have on vibrational coupling between the two modes, and may also be involved in the unusually fast vibrational relaxation rate observed in heme proteins.

A number of studies analyzing the process of heme and CO ligand cooling,[4,5,8,20,21] as well as assigning the key vibrational modes of Fe in the MbCO vibrational spectrum,[22] have been carried out. The MbCO infrared pump−probe measurements of Hill et al.[21] and of Hochstrasser et al.[20] in solvated MbCO, HbCO, and a protoheme system measure ultrafast (picosecond time scale) cooling rates for the vibrationally excited CO ligand. The excited state relaxation time of MbCO was found to be $T_1 = 17$ ps, significantly faster than is typical for metal carbonyls,[23] with $W(CO)_6$ in CCl_4 ($T_1 = 800 \pm 200$ ps), $Cr(CO)_6$ in $CHCl_3$ ($T_1 = 295 \pm 30$ ps), and $Ir(CO)Cl(TPP)_2$ ($T_1 = 50 \pm 13$ ps). The relaxation time decreases with increasing molecular complexity, as a result of the increased number of internal vibrational modes available for coupling. Relaxation times in heme proteins systems are therefore faster than in protoheme complexes (31 ps). Interaction with the solvent also influences the vibrational cooling rate, although to a lesser extent.[20]

Recent experimental results of Mizutani[8] examined cooling of the photodissociated MbCO heme group and CO ligand immediately after photodissociation takes place. Their analysis helped to confirm the predictions of the earlier theoretical studies of Henry,[7] who used MD simulations to model heme cooling after photoexcitation. A two-stage cooling process was predicted, with an initial fast cooling rate (decay constant 1−4 ps) that was found to be in good agreement with experimental values (time constant 2 ps).[8] The subsequent, slower cooling phase was found experimentally to consist of two subcomponents, a faster component with a time constant of 7.5 ps, followed by a slower component with a time constant of 20 ps. The MD results, however, tended to overestimate the relaxation time of both of these slower steps, probably as a result of neglecting solvent molecules during the simulation. It is believed that the slow component arises from energy transfer from the heme to the surrounding solvent, while the very fast initial heme cooling rates arise from coupling within the molecule.[8]

Associated spectroscopic data are also available, allowing accurate vibrational analysis of the bound heme system. For example, nuclear resonance vibrational spectroscopy (NRVS) measurements recently assigned the major Fe vibrational frequencies in MbCO.[22] Such measurements provide a useful reference when fitting force field parameters, ensuring that the bond force constants support realistic vibrational frequencies for the system.

For heme cooling, harmonic bonded terms and classical MD techniques have proven sufficient to provide realistic behavior.[7,8] Difficulties are likely to arise when the difference in vibrational frequency between two coupled vibrational modes becomes large, and anharmonic coupling becomes relevant. IR measurements found the A_1 substate of bound CO in MbCO at $\approx$1949 cm^{-1}.[24] This value is substantially larger than that of the adjacent Fe−C_{CO} bond ($\approx$507 cm^{-1})[22] or FeCO bending mode (modes ranging from 561 to 589 cm^{-1}),[22] but the system still exhibits rapid CO cooling in pump−probe experiments.[20] This fast vibrational relaxation of the CO ligand despite a significant difference in vibrational frequency between the CO bond and adjacent vibrational modes is challenging to characterize using force fields in MD simulations, as will be demonstrated here. In the current work, we address the following questions: What are the limitations of harmonic interaction potentials? Is it possible to describe relaxation rates *and* vibrational frequencies with the same force field? What role do electrostatic interactions play in describing vibrational effects in MbCO, and finally, does inclusion of correlated Fe−C_{CO} and CO bond strengths affect relaxation time in MD simulations?

II. Methods

A. Details of Molecular Dynamics Simulations. MD simulations were carried out using the CHARMM program,[25] and the CHARMM22 force field.[26] The MbCO structure was taken from the X-ray study of Kuriyan et al.[27] (Protein Data Bank reference 1mbc), with hydrogen atoms added within CHARMM. The $His_\epsilon 64$ tautomer was used throughout.[28,29] A region of the protein centered at the binding site was solvated using three overlays of a 16 Å sphere of equilibrated water molecules. The remainder of the protein was left unsolvated to improve computational efficiency,[30,31] as the dynamics of the bound ligand and heme in the active site are the focus of this study. The stochastic boundary method was used,[32] with a solvent

boundary created with a radius of 16 Å to constrain the water molecules. An inner sphere was defined with a radius of 12 Å centered on the heme group, inside which the system was propagated using Newtonian dynamics with a time step of 1 fs. In the buffer region between 12 and 16 Å, the system was propagated using Langevin dynamics. In total, 2534 protein and ligand atoms were included in the system and 178 water molecules. Water molecules were represented with a TIP3P potential. Unless otherwise stated, gas phase CO charges of 0.021 *e* and −0.021 *e* were used for the bound ligand C and O atoms, respectively, as charges for bound CO were not found among the standard CHARMM22 force field parameter set. The effect of altering CO charges on CO relaxation time is described in the text. Nonbonded interactions were truncated at a distance of 9 Å. Friction coefficients of 62 and 250 ps^{-1} were applied to water molecule oxygen atoms and remaining non-hydrogen atoms in the remainder of the system, respectively. All bonds to hydrogen atoms were constrained using the SHAKE algorithm.[33] The entire system was equilibrated at 300 K for 90 ps. Trajectories were typically 80 ps in length, with CO excitation taking place after the first 10 ps of simulation time. Twenty such trajectories were averaged to obtain reliable vibrational relaxation rates. Some trajectories were extended to 800 ps where slow CO cooling rates were encountered. At least six such trajectories were averaged for each set of CO parameters to improve sampling. Photodissociated CO was modeled using the "sudden approximation"[34] with gas phase CHARMM22 bond force constants and atomic charges.

The C−O bond was vibrationally excited to the $v = 1$ state by compressing the bond to increase the internal energy by 5.73 kcal/mol (24 kJ/mol). This corresponds to the energy of an absorbed photon from a 5 μm laser pulse, used in the pump−probe experiment of Hochstrasser et al.[20] Energy dissipation away from the excited C−O bond was then followed by monitoring the bond length and associated vibrational energy as a function of time (eq 1). The averaged vibrational energy over all simulations as a function of simulation time provides the vibrational cooling curve. Averaging was carried out in two stages. The CO bond vibrational energy fluctuates rapidly with time due to collisions and coupling to internal modes in the surrounding protein. The time average is therefore a more informative measure of bond energy than instantaneous values. The vibrational energy was preaveraged over 200 fs time windows. The resulting cooling curves were then averaged over all trajectories, and the vibrational relaxation times, T_1, are calculated according to eq 1 by fitting $T_1(t)$ to a decaying exponential.

For the vibrational spectra, the real-time dipole−dipole autocorrelation function, $C(t)$, is calculated. The power spectrum, $C(\omega)$, is computed from the Fourier transform of $C(t)$.[35] To construct $C(t)$, the dipole moment (for CO), the Fe−C_{CO} bond length (for FeC), and the FeCO angle are recorded at 2^n consecutive time steps, typically corresponding to the last 524 ps (2^{19} time steps) of an 800 ps trajectory, or 65.5 ps (2^{16} time steps) of an 80 ps trajectory. The resulting data are then transformed via Fourier transform with a Blackman filter.[36] The infrared spectrum (for CO) or the power spectra (for FeC and FeCO) are calculated using

$$A(\omega) = \frac{c_0\omega}{3\hbar}(1 - \exp(-\hbar\omega/(k_B T)))C(\omega) \qquad (3)$$

where k_B is the Boltzmann constant, $c_0 = 4\pi^2/(cn)$ (with c being the speed of light and n the refractive index), and T is the temperature.[35,37] Resulting spectra are then averaged over six or more trajectories. Both the Fe−C_{CO} and C−O stretch frequencies are then clearly visible in the resulting spectrum.

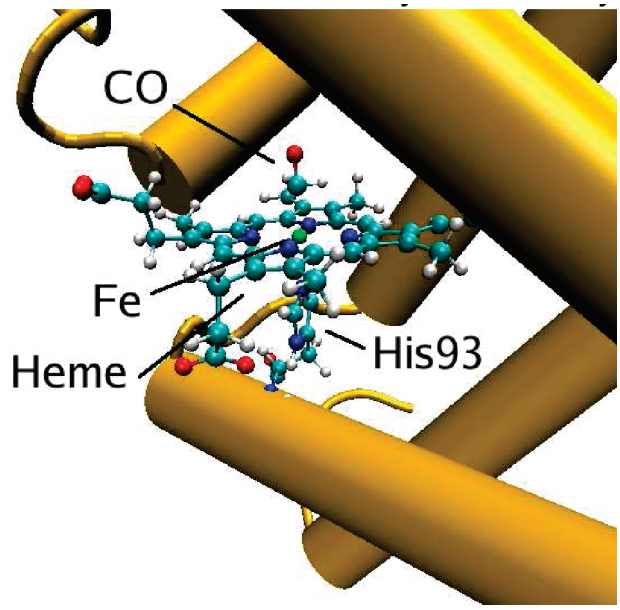

Figure 1. MbCO complex showing heme, CO, and His93 moieties used as a model system for DFT calculations.

B. Automated Parameter Fitting. In the following, average relaxation rates (from a number of independent MD trajectories) and vibrational spectra are our target data which we wish to best describe given a particular force field parametrization. This eventually leads to an involved fitting problem which was addressed by using an interface[38] between CHARMM and the I-NoLLS[39] fitting environment. Within this framework, measured quantities such as vibrational frequencies and relaxation rates are treated as observables (y variables) in I-NoLLS. Values to be fitted, such as Morse potential parameters and bond force constants, are passed as x variables. Each parameter optimization cycle then involves running MD simulations within CHARMM to obtain the calculated y values corresponding to a given set of x values suggested by I-NoLLS.

C. Quantum Chemical Calculations. Density functional theory (DFT) calculations were used to obtain the anharmonic bond energy profiles required for the CO and Fe−C_{CO} Morse potentials. All electronic structure calculations were performed using the Gaussian 03 suite of programs[40] and the hybrid B3LYP functional.[41,42] The heme group, bound CO, and proximal His93 residue were included explicitly in each DFT calculation (Figure 1). A VDZ basis set[43] was used for the CO ligand and Fe and N atoms, while the remaining atoms were described with the smaller 3-21G basis set. B3LYP geometry optimizations were performed on the Fe−C_{CO} and C−O bonds, and potential energy scans were carried out for the CO and Fe−C_{CO} bonds. The energies were then fitted to a Morse function $V(r) = D_e(1 - \exp(-\beta(r - r_{eq})))^2$, where V is a function of bond length r, bond dissociation energy D_e, equilibrium bond length r_{eq}, and the steepness parameter β. Both optimized bonds were lengthened and contracted five times at 0.025 Å intervals while freezing all other internal coordinates, giving a total of 11 sampled bond lengths r for each bond, centered at the equilibrium distance r_{eq}.

A relaxed two-dimensional potential energy surface $V(r_{CO},r_{FeC})$ with 121 points was calculated by sampling CO bond energy profiles at 11 different fixed FeC_{CO} bond lengths. Morse potential parameters and harmonic bond force constants were

fitted for each CO energy profile to determine their dependence on the FeC_{CO} bond length. An analogous potential energy surface was then fitted by sampling FeC_{CO} bond energy profiles at 11 fixed CO bond lengths.

The two-dimensional energy surface described above was used to obtain a fluctuating bond-force-constant model (model I) which was then implemented into CHARMM. Linear expressions for the variation of the Fe−C_{CO} and CO harmonic force constants as a function of the length of the neighboring bond were fitted according to

$$k_\alpha(r_\beta) = a + br_\beta \quad (4)$$

with k_α being the harmonic force constant of bond α = CO (or Fe−C_{CO}) as a function of the bond length r of its neighbor β = Fe−C_{CO} (or CO). a and b are parameters fitted from the intercept and gradient of the linear relationship, respectively. For quadratic interactions, the total bonded energy of the Fe−C_{CO} and CO bonds then is

$$V(r_{CO}, r_{FeC}) = k_{CO}(r_{FeC})(r_{CO} - r_{CO,eq}(r_{FeC}))^2 + k_{FeC}(r_{CO})(r_{FeC} - r_{FeC,eq}(r_{CO}))^2 \quad (5)$$

where $r_{CO,eq}$ is the equilibrium bond length of the CO bond.

To assess the influence of harmonic interactions in this 2D potential, a second model (model II) was parametrized using linear expressions (analogous to eq 4) for the variation of the Morse parameters (D_e, r_{eq}, and β). The total bonded energy then is

$$V(r_{CO}, r_{FeC}) = D_e^{FeC}(r_{CO})(1 - \exp(-\beta_{FeC}(r_{CO})(r_{FeC} - r_{FeC,eq})))^2 + D_e^{CO}(r_{FeC})(1 - \exp(-\beta_{CO}(r_{FeC})(r_{CO} - r_{CO,eq})))^2 \quad (6)$$

It should be noted that D_e is a parameter here (and not fixed at experimental values that are not always available), as the aim of fitting to a Morse potential is to accurately represent the bond energy profile around its equilibrium bond length, and the Fe−C_{CO} and CO bond lengths never approach dissociation in these simulations.

III. Results and Discussion

In the following, the models are explored to better characterize and understand how vibrational relaxation times and vibrational spectroscopy depend upon the potential energy functions used. In particular, the effect of harmonic potentials compared to anharmonic Morse functions and that of uncoupled and coupled vibrational stretching and bending modes in influencing the vibrational relaxation rate of the excited CO ligand is discussed.

A. Harmonic Bonded Terms. The cooling curves resulting from six 800 ps trajectories with standard CHARMM22 harmonic bonded force constants for the CO and Fe−C_{CO} bonds are shown in Figure 2a. The resulting averaged CO cooling time of T_1 = 432 ps is much slower than the experimental value[20] of 17 ps. Indeed, the cooling rate of the bound ligand is reminiscent of that obtained from simulations of photodissociated CO, with CO in the binding pocket (Figure 1) shown as the red curve in Figure 2a, and that of the measured[44] photodissociated cooling CO time (T_1 = 600 ± 150 ps). It seems that essentially no coupling takes place between C−O and the adjacent heme

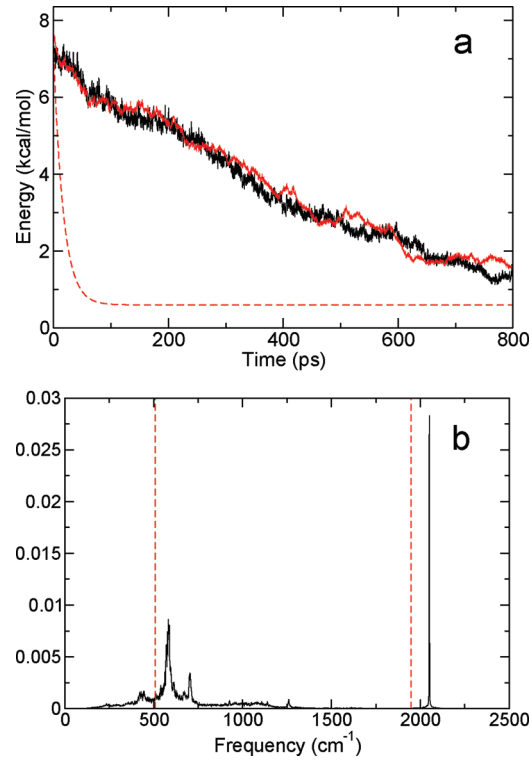

Figure 2. (a) Vibrational relaxation of the CO bond in bound (black) and photodissociated (red) MbCO. An exponential decay curve with the experimental cooling constant T_1 = 17 ps is shown for reference as a red dashed line. (b) Vibrational spectrum of the bound system showing CO and Fe−C_{CO} vibrational frequencies. Standard CHARMM22 harmonic bond force constants are used to describe both systems. The red dashed lines mark the positions of experimental spectral peaks.

vibrational modes in these simulations. In contrast to previous MD studies of heme vibrational relaxation,[5−7] which accurately modeled vibrational cooling of photoexcited heme using harmonic bonded parameters, use of harmonic bonded terms to model the bound CO ligand in MbCO is inadequate to investigate vibrational relaxation. As discussed earlier, this is likely to arise from the large separation in vibrational frequency between CO and the surrounding vibrational modes, leading to inefficient coupling between the oscillators. The corresponding vibrational spectrum is shown in Figure 2b. There is reasonable agreement with experimental IR frequencies, although the Fe−C_{CO} stretch is blueshifted to around 580 cm^{-1} from the experimental value[22] of 507 cm^{-1}, and the CO stretch is blueshifted to around 2050 cm^{-1} from the experimental value[24] of around 1949 cm^{-1} for the MbCO A_1 substate.

B. Morse Potential for CO. Using a Morse potential for the CO bond is expected to increase the available density of states and may allow coupling with the Fe−C_{CO} bond (harmonic). The Morse parameters were obtained as described in the Methods section, although the β parameter was adjusted slightly to yield realistic CO vibrational frequencies in MD trajectories: D_e = 260.6 kcal/mol, r_e = 1.128 Å (from DFT calculations), and β = 1.984 $Å^{-1}$. The cooling time averaged over 20 trajectories (black curve in the left-hand side of Figure 3a) is T_1 = 340 ps, very slow but nonetheless faster than the harmonic model. The associated vibrational spectrum is shown in the left-hand side of Figure 3b, with a C−O stretch of 1976 cm^{-1} and a blueshifted Fe−C_{CO} stretch of around 580 cm^{-1}, similar to the harmonic model and in reasonable agreement with experimental measurements.

The CO relaxation time was found to depend on the mismatch between CO and Fe−C_{CO} frequencies. Increasing the Fe−C_{CO}

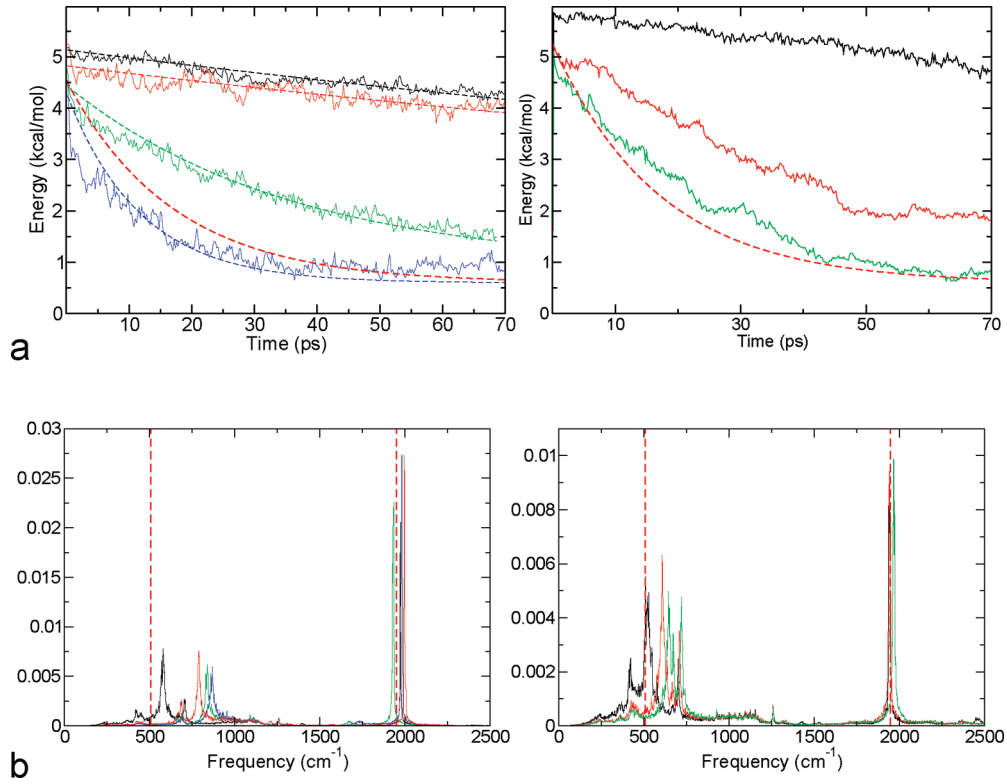

Figure 3. (a) Left: Vibrational relaxation of the CO bond in simulations using harmonic Fe−C_{CO} parameters and a Morse potential for the C−O bond. Fitted exponential decay curves used to estimate T_1 are overlaid as dashed lines. The Fe−C_{CO} harmonic force constant is varied between 258 (black), 558 (red), 758 (green), and 858 (blue) kcal mol^{-1} Å^{-2} to show the effect on CO vibrational cooling rate. Simulations with a force constant of 858 kcal mol^{-1} Å^{-2} applied to the Fe−C_{CO} bond required reduction of the Morse β parameter from 1.984 to 1.644 Å^{-1} to maintain an accurate CO vibrational frequency. Right: Cooling of the CO bond with Morse potentials for both the Fe−C_{CO} and CO bonds. The Fe−C_{CO} β Morse parameter is varied to show the effect on vibrational cooling rate, while the CO β parameter is adjusted to maintain a constant CO stretch frequency. Vibrational relaxation curves from trajectories with $\beta_{Fe-C} = 2.9$ and $\beta_{CO} = 2.1$ (black), $\beta_{Fe-C} = 3.7$ and $\beta_{CO} = 2.1$ (red), and $\beta_{Fe-C} = 4.1$ and $\beta_{CO} = 2.2$ (green) are shown. An exponential decay curve with the experimental cooling constant $T_1 = 17$ ps is shown as the lower red dashed line. (b) Left: Corresponding harmonic Fe−C_{CO} vibrational spectra, with the same color scheme as part a. Right: Vibrational spectra of C−O and Fe−C_{CO} bonds using Morse potentials. The colors match the corresponding cooling curves in part a. The red dashed lines mark positions of experimental spectral peaks.

harmonic force constant, k_{FeC}, increases the Fe−C_{CO} vibrational frequency and decreases the mismatch, gradually leading to faster vibrational cooling; additionally, the CO stretch also shifts to higher frequencies, although to a lesser extent. To allow better comparison between cooling rates using the different models, in the following, the CO β parameter is adjusted for each value of the Fe−C_{CO} force constant k_{FeC} to maintain the CO vibrational frequency close to the experimental value of 1949 cm^{-1}. The decrease in CO cooling time toward the experimental value therefore comes at the expense of the accuracy of the Fe−C_{CO} stretch frequency.

A substantial increase in the k_{FeC} force constant is required before efficient vibrational coupling can take place with the CO stretch. An increase from 258 to 558 kcal/mol Å^{-2}, for example, is too small to enable efficient coupling, and leads to little change in cooling time with $T_1 = 340$ ps. Large force constants of $k_{FeC} = 758$ kcal/mol Å^{-2} are required to allow substantially faster cooling times ($T_1 = 42$ ps), and not until $k_{FeC} = 858$ kcal/mol Å^{-2} is very rapid cooling possible ($T_1 = 11.7$ ps, Figure 3a). The latter value of k_{FeC} correspondingly reduces the accuracy of the Fe−C_{CO} stretch frequency by blueshifting to 855 cm^{-1} (Figure 3b). The CO stretching frequency is maintained at 1958 cm^{-1}, with the spectrum shown in Figure 3b.

Similar decreases in vibrational cooling time are reached by fixing the Fe−C_{CO} force constant and decreasing β_{CO}. It was found to be a general rule that faster cooling times are obtained by reducing the separation in the vibrational frequencies of CO and strongly coupled local modes. The rapid change in T_1 between 758 and 858 kcal mol^{-1} Å^{-2}, despite a relatively small change in spectroscopy, demonstrates that, once coupling becomes efficient, cooling time is very sensitive to small parameter changes or, stated differently, once the vibrations are coupled the problem becomes a meaningful fitting problem. Different models and parameter sets were therefore explored to characterize the problem and achieve both accurate spectroscopy and vibrational cooling time.

C. Fe−C_{CO} and C−O Morse Potentials. As combining a Morse potential for the CO bond with a harmonic potential for the Fe−C bond did not provide sufficient coupling between the modes to achieve both accurate cooling times and vibrational spectra simultaneously, an ansatz with Morse potentials for both modes was next pursued. Introducing a second Morse potential for the Fe−C_{CO} bond is expected to similarly increase the density of states in this bond to provide more efficient coupling with the Morse potential of CO. The fitted Fe−C_{CO} Morse parameters were $D_e = 23.02$ kcal/mol, $r_e = 1.746$ Å, and $\beta = 2.904$ Å^{-1}, with D_e in good agreement with the experimental binding enthalpy of CO in MbCO of -21.4 ± 0.3 kcal/mol.[45] The CO Morse parameters then needed to be slightly modified to $D_e = 230.0$ kcal/mol and $\beta = 2.1$ Å^{-1} to maintain a realistic CO vibrational frequency as before. The averaged cooling curve from 20 trajectories using these parameters is shown in black in the right-hand side of Figure 3a, and has a cooling time of $T_1 = 321$ ps. The vibrational frequency is in good agreement

with experiment (Figure 3b), with an Fe−C_{CO} stretch of around 510 cm^{-1} and a CO stretch of around 1944 cm^{-1}. This represents a similar cooling time to the trajectories using a harmonic bonded potential for the Fe−C_{CO} bond. Again, the sensitivity of T_1 and the vibrational spectroscopy to the Morse parameters is considered: with $\beta_{FeC} = 3.7$ $Å^{-1}$, the cooling time is reduced to $T_1 = 47$ ps (red in the right-hand side of Figure 3a) and the Fe−C_{CO} stretch frequency is blueshifted from 510 to 608 cm^{-1}, whereas, for $\beta_{FeC} = 4.1$ $Å^{-1}$, the cooling time is reduced to $T_1 = 23.1$ ps (green in the right-hand side of Figure 3a) and the Fe−C_{CO} stretch frequency is blueshifted to 645 cm^{-1}, over 100 cm^{-1} closer to the experimental value than needed for a similar cooling time with a harmonic Fe−C_{CO} potential. It is clear, however, that using a Morse potential for both the CO and Fe−C_{CO} bonds does not lead to fast vibrational cooling without a substantial shift of the vibrational frequency.

D. The FeCO Bending Mode. Strong dependence of the CO relaxation time on the FeCO angular force constant has also been observed (Figure 4a). Morse potentials were again used for the CO and Fe−C_{CO} bonds, with parameters chosen to accurately represent the experimental CO and Fe−C_{CO} bond stretch frequencies. The FeCO force constant has to be increased from 35 kcal mol^{-1} rad^{-2} (black curve, $T_1 = 322$ ps) to 55 kcal mol^{-1} rad^{-2} before a decrease in cooling time to $T_1 = 97$ ps (red curve) is reached. A further increase to 75 kcal mol^{-1} rad^{-2} (green curve) is needed before very fast cooling ($T_1 = 12$ ps) is possible. Interestingly, when a harmonic Fe−C_{CO} bonded term is used in conjunction with an FeCO angular force constant of 75 kcal mol^{-1} rad^{-2}, a slower cooling time of $T_1 = 48$ ps results for the same Fe−C_{CO} and CO vibrational frequencies. This suggests that the Fe−C_{CO} Morse potential to some extent increases the efficiency of coupling to the FeCO bending mode. In contrast to fitting Morse potentials for the Fe−C_{CO} and CO stretching modes, fitting an anharmonic FeCO bending term to DFT data to introduce an anharmonic bending function into CHARMM did not significantly decrease the CO relaxation time.

The CO and Fe−C_{CO} vibrational frequencies remain largely unchanged by altering the FeCO angular force constant (Figure 4b). The cost in accuracy to the FeCO bending frequency, however, is an increase from 602 cm^{-1} at 35 kcal mol^{-1} rad^{-2} (black spectrum in Figure 4c) to 704 cm^{-1} at 75 kcal mol^{-1} rad^{-2} (green spectrum). This blueshift of 129 cm^{-1} from the experimental value of 575 cm^{-1} is substantial but similar to the shifts in Fe−C_{CO} vibrational frequency required for the Morse−Morse model to achieve a similar cooling rate.

No further bending or vibrational modes were found to strongly affect the CO vibrational relaxation time. Indeed, considering the energy flow away from the CO bond into surrounding modes showed that energy transfer into the Fe−C_{CO} stretching mode is the rate determining step, with energy then dissipating very rapidly away into other surrounding modes (Figure 5). Figure 5a shows a gradual increase in velocities of local heme carbon and nitrogen atoms, averaged over 20 trajectories, and after CO excitation. All atoms, however, seem to share roughly the same velocity increase, suggesting a fairly even distribution of energy between modes. The total increase in energy in the heme group (including N_ϵ of His93) after energy has been added to CO (10 ps into the trajectory) is seen to be roughly 1 kcal/mol. This is despite CO losing around 3.5 kcal/mol over the same period, showing rapid heme cooling must take place to remove the excess energy. This fast heme cooling rate is in agreement with previous experimental and theoretical results, which suggest that heme cooling takes place on a very

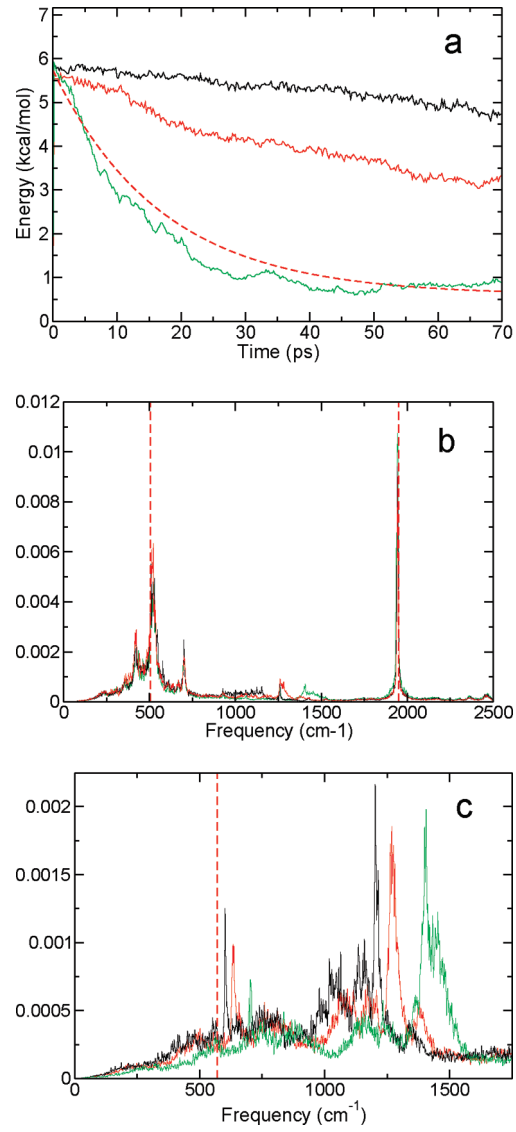

Figure 4. (a) Cooling of the C−O bond with Morse potentials on Fe−C_{CO} and C−O bonds. The Fe−C−O angular force constant is increased from the CHARMM22 value of 35 kcal mol^{-1} rad^{-2} (black) to 55 kcal mol^{-1} rad^{-2} (red) and 75 kcal mol^{-1} rad^{-2} (green) to demonstrate the effect on CO cooling rate. An exponential decay curve with the experimental cooling constant $T_1 = 17$ ps is shown for reference as a red dashed line. (b) Vibrational spectra of C−O and Fe−C_{CO} bonds, with the colors and force constants corresponding to the cooling curves in part a. The red dashed lines mark the positions of experimental spectral peaks. (c) Vibrational spectra of the FeCO bending mode, with the angular force constants again corresponding to those of the cooling curves in part a. The red dashed line marks the position of the experimental spectral peak.

fast time scale with energy immediately redistributed to peripheral heme groups and not concentrated in internal modes.[7,8] Initial energy transfer to the Fe−C_{CO} bond is then the rate determining step, with remaining modes providing part of a network to quickly disperse energy over a large number of atoms, at least within a classical MD framework. The faster vibrational cooling rate with increasing FeCO angular force constant, despite no visible energy build-up in the FeCO bending mode, might suggest that the role of the bending mode is to hold the Fe−C_{CO} and CO bonds more collinear to improve coupling between them. It could also be, however, that energy is transferred directly into, and then very rapidly away from

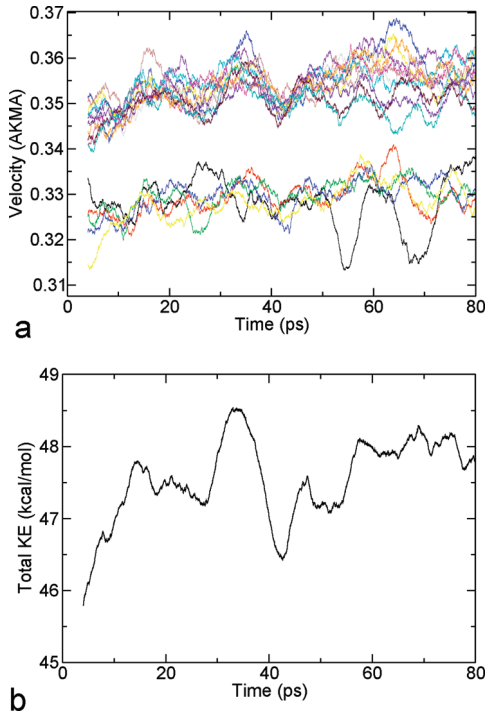

Figure 5. (a) Running averages of velocities (in AKMA units of Å/0.0489 ps) of local heme and His93 carbon (series with higher velocities) and nitrogen (series with lower velocities) atoms. Data are averaged over 20 trajectories. (b) Running average of total heme kinetic energy (kcal/mol), obtained by summation over instantaneous velocities of all heme atoms and N_ϵ of His93 throughout the trajectories. Data are averaged over 20 trajectories.

the FeCO bending mode, making FeCO directly involved in energy transfer from CO or Fe−C_{CO} to surrounding heme modes.

The relaxation times are largely insensitive to force field parameters for modes other than Fe−C_{CO} and FeCO. For example, heme doming modes, implicated in the relaxation mechanism of the related MbCN system,[9] are found to be of minor influence. A relatively slow relaxation time of $T_1 = 142$ ps is reached by increasing the Fe−N_{His} bond force constant from 65 to 325 kcal mol^{-1} Å^{-2}, with Morse potentials used to describe the Fe−C_{CO} and CO bonds. The out-of-heme-plane Fe−Im vibrational frequency is strongly affected by making such a change, with frequencies shifted from 220 to 365 cm^{-1}. Indeed, the Fe−C_{CO} vibrational frequency is also affected by the change, so it may actually be the impact on Fe−C_{CO} frequency that is responsible for the moderate decrease in cooling time observed. Greater sensitivity of CO relaxation time to the N_{porph}−Fe−C_{CO} angular force constant exists, as increasing from 50 to 95 kcal mol^{-1} rad^{-2} allows a cooling time of $T_1 = 98$ ps. The change is accompanied by a significant change in FeCO bending frequency, however, which is likely to be responsible for the faster relaxation.

E. Role of Nonbonded Interactions in CO Relaxation. Finally, the role of electrostatic interactions in the relaxation of the CO bond was considered. The C and O force field point charges were increased from their standard CHARMM22 values of ±0.021 *e* to ±0.21 *e* and ±0.41 *e*, respectively, to determine whether stronger electrostatic interactions would allow more efficient coupling. Morse potentials were used for the CO ($\beta = 2.1$ Å^{-1}) and FeC_{CO} ($\beta = 2.904$ Å^{-1}) bonds, with parameters that provide accurate experimental IR frequencies, and the corresponding cooling times were largely unaffected. They changed from the initial $T_1 = 432$ ps with $q_C = 0.021$ *e* to 437 ps with $q_C = 0.21$ *e* and 437 ps with $q_C = 0.41$ *e*. The small impact of this change in atomic charges, within the error associated with the method, suggests that cooling via nonbonded electrostatic interactions is inefficient. This is in agreement with the findings of previous work on diatomic molecules in liquids.[18] It therefore seems that fast vibrational relaxation on the $T_1 = 17$ ps time scale takes place primarily via coupling to local bonded vibrations. However, given that some dependence of the relaxation rate on the details of the electrostatic interactions was found in other systems,[3,16] no general conclusion can be made as yet about differences among systems where electrostatic interactions are or are not significant for vibrational relaxation. It should, however, be noted that the largest differences in these examples were found between simulations with or without electrostatics; once electrostatics was included, differences in the relaxation times became smaller.[3]

F. Electronic Effects: Fluctuating Force Constants. The data presented so far demonstrate that, within classical dynamics, coupling of vibrational modes is the major factor that affects the CO cooling rate. Until now, electronic effects—most notably Fe−C_{CO} backbonding—have not yet been considered. It is well-known that the strength of the Fe−C_{CO} bond depends on the bond length of the CO bond, and vice versa, as bond stretching affects orbital overlap.[19] One way to capture such effects is to use bond potentials in which the force constant or Morse parameters of one bond depend on the length of the other (see Methods). The parameters for both the fluctuating harmonic force constant (model I) and fluctuating Morse (model II) models are given in Table 1. The dependence of bond energy profiles of each bond on its neighbor is obtained from DFT results, while harmonic force constants and Morse β parameters are altered slightly to maintain accurate experimental vibrational frequencies.

Cooling curves and vibrational spectra obtained using model I are shown in Figure 6. Such an approach does not lead to rapid CO cooling, even when the a_{FeC} parameter (eq 4) is increased from −100.7 kcal mol^{-1} Å^{-2} ($T_1 = 303$ ps) to 99.3 kcal mol^{-1} Å^{-2} ($T_1 = 250$ ps), creating a systematic shift in the fluctuating harmonic force constant of 200 kcal mol^{-1} Å^{-2}, and a corresponding shift in the vibrational spectrum (Figure 6b). The parameters b_{CO} and b_{FeC} were kept fixed so that the fluctuation of bond strength with length of the neighboring bond remained within values suggested by the DFT data. The ansatz, then, leads to slow cooling times, although faster than a conventional harmonic bond force constant model (left side of Figure 2a, $T_1 = 432$ ps).

Model II leads to cooling curves shown in Figure 6a. In this model, the equilibrium bond length is also allowed to fluctuate as a function of the length of the neighboring bond. The use of Morse potentials in place of harmonic bond potentials leads to more efficient coupling and faster cooling times than were achieved using model I. As the parameters a_{CO} and a_{FeC} (eq 4) are altered, however, fast cooling ($T_1 = 28$ ps) is not observed without introducing a shift in the Fe−C_{CO} vibrational frequency of 117 cm^{-1} (Figure 6b). The performance of model II therefore remains similar to that obtained using Morse potentials with fixed parameters for the CO and Fe−C_{CO} bonds (right side of Figure 3).

Introducing correlated bonded potentials in this way into MD simulations does not facilitate energy transfer between bonds to significantly affect the vibrational relaxation rate. It is possible, however, that increasing the dimensionality of the fitted surface further, for example by introducing correlation of bonded parameters between the CO, Fe−C_{CO}, and Fe−N_{His} bonds, would increase the efficiency of CO vibrational cooling.

TABLE 1: Table Listing Fluctuating Harmonic Force Constant (Model I) and Morse Potential (Model II) Parameters[a]

model	$a_{\beta_{CO}(k_{CO})}$	$b_{\beta_{CO}(k_{CO})}$	$a_{D_{e,CO}(k_{FeC})}$	$b_{D_{e,CO}(k_{FeC})}$	$a_{r_{eq,CO}}$	$b_{r_{eq,CO}}$	$a_{\beta_{FeC}}$	$b_{\beta_{FeC}}$	$a_{D_{e,FeC}}$	$b_{D_{e,FeC}}$	$a_{r_{eq,FeC}}$	$b_{r_{eq,FeC}}$
model I	1400	−160.31	−100.7	274.2								
model II	−1.045	1.381	1152.8	−389.2	1.060	0.034	2.915	−0.231	−36.909	56.744	2.299	−0.422

[a] All values are reported in CHARMM AKMA units, with distances in Å and energies in kcal mol^{-1}. Parameters correspond to linear expressions based on eq 4. Parameter subscripts in brackets refer to model I.

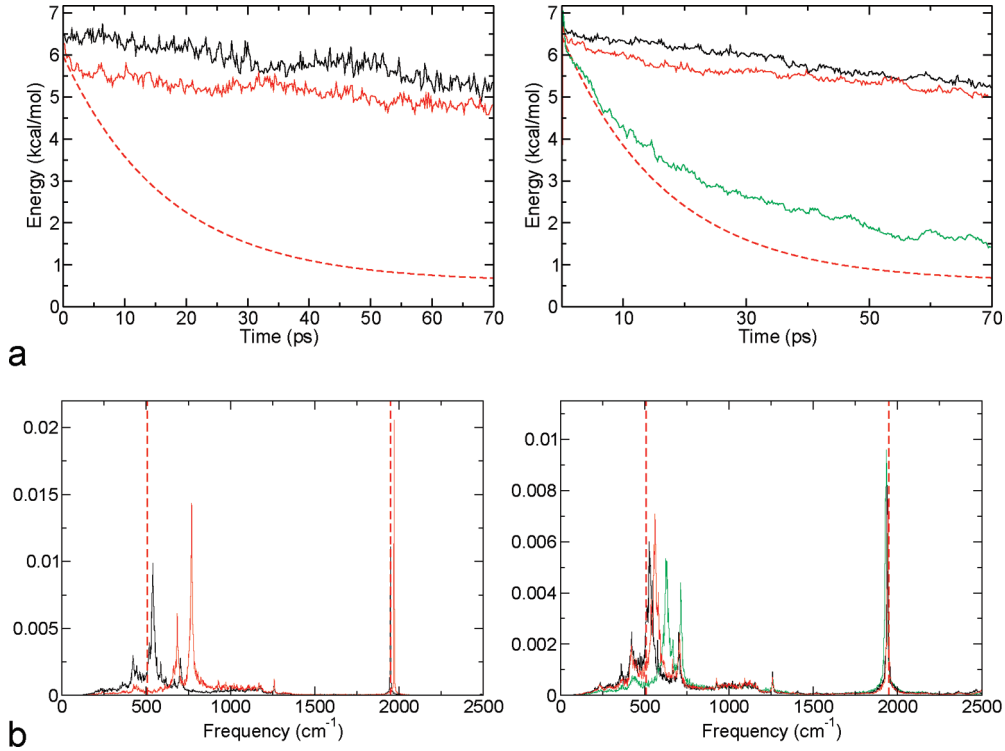

Figure 6. (a) Left: CO relaxation curves using the fluctuating harmonic force constant model (model I). Results using a_2 values of −100.7 (black) and 99.3 (red) kcal mol^{-1} Å^{-2} are shown. Right: CO relaxation curves using the fluctuating Morse potential model (model II). Results using a_1 and a_4 values of −1.04 and 2.91 Å^{-1} (black), −1.04 and 3.31 Å^{-1} (red), and −1.05 and 3.61 (green) Å^{-1} are shown. An exponential decay curve with the experimental cooling constant $T_1 = 17$ ps is shown in both figures for reference as a red dashed line. (b) Left: Vibrational spectra of Fe−C_{CO} and CO bonds using model I with a_2 values of −100.7 (black) and 99.3 (red) kcal mol^{-1} Å^{-2}. Right: Vibrational spectra of Fe−C_{CO} and CO bonds using model II with corresponding a_1 and a_4 values labeled using the same colors as in part a. The red dashed lines mark the positions of experimental spectral peaks.

IV. Fitted Parameters

Finally, a model was fitted by simultaneously optimizing CO and FeC_{CO} Morse parameters and the FeCO angular force constant according to the procedure outlined in the Methods section. The goal was to include the coordinates that most influence the vibrational relaxation rate in a fit that yields fast cooling times and best captures the vibrational spectroscopy of the system. The β_{CO} and β_{FeC} Morse parameters and k_{FeCO} angular force constant were optimized to the values reported in Table 2, leading to a new model with $T_1 = 50$ ps. The CO and FeC_{CO} stretch frequencies and FeCO bending mode frequency are all within 45 cm^{-1} of their experimental values, of similar or slightly greater accuracy than the original CHARMM model. While the cooling time is 33 ps above the experimental value of 17 ps, it is much faster than the value of 432 ps achieved using a traditional harmonic force field approach with CHARMM22 parameters (Figure 2). Cooling times faster than 50 ps can be achieved, but the vibrations will be described less accurately. The overall performance of this model in relation to all other models described so far can be seen in Table 2. The fitted model seems to offer a good compromise, providing both accurate spectroscopy and reasonably fast vibrational relaxation rates. Including other local degrees of freedom in a much wider fit to fully account for the normal modes of the entire heme system may be one way to improve the model further.[22]

V. Discussion and Conclusions

The present work establishes that conventional force fields based on harmonic bonded potentials which are able to provide accurate vibrational spectra can be inappropriate when considering energy transfer between vibrational modes with widely separated frequencies. As well as having implications for nonequilibrium MD simulations with locally excited vibrational modes, this result may also affect the suitability of classical MD simulations to investigate allosteric communication pathways in protein simulations, known to be related to energy transfer pathways.[1,2]

In MbCO, the system studied here, it was found that rapid vibrational relaxation of the CO ligand takes place primarily via coupling to local vibrational modes, rather than through nonbonded interactions. The Fe−C_{CO} stretch and FeCO bending modes were identified as particularly important to vibrational cooling of CO on a realistic time scale. Introduction of Morse potentials to both the CO and Fe−C_{CO} bonds improves coupling between these modes, and provides faster CO cooling times with a smaller impact on vibrational frequencies. Other local modes

TABLE 2: Table Comparing the Performance of Different Models and Parameter Combinations Reported in the Text[a]

model	$\delta\nu_{Fe-C}$	$\delta\nu_{CO}$	$\delta\nu_{FeCO}$	$\delta(\nu_{CO}-\nu_{FeC})$	T_1
harmonic	75	104		29	432
CO Morse, Fe−C_{CO} harm.					
$\beta_{CO} = 1.984$, $k_{FeC} = 258$	72	26		−46	340
$\beta_{CO} = 1.884$, $k_{FeC} = 758$	331	−16		−347	42
$\beta_{CO} = 1.644$, $k_{FeC} = 858$	350	9		−341	12
CO Morse, Fe−C_{CO} Morse					
$\beta_{CO} = 2.1$, $\beta_{FeC} = 2.9$	6	−8		−14	321
$\beta_{CO} = 2.1$, $\beta_{FeC} = 3.7$	103	−8		−111	47
$\beta_{CO} = 2.2$, $\beta_{FeC} = 4.1$	141	19		−122	23
FeCO bending					
$k = 35$	6	0	32	−6	322
$k = 55$	6	0	64	−6	97
$k = 75$	6	0	134	−6	12
fluct. harm. (model I)					
$a_{k_{FeC}} = -100.7$	32	1		−31	303
$a_{k_{FeC}} = 99.3$	264	22		−242	250
fluct. Morse (model II)					
$a_{\beta_{CO}} = -1.04$, $a_{\beta_{FeC}} = 2.91$	19	−9		−28	281
$a_{\beta_{CO}} = -1.04$, $a_{\beta_{FeC}} = 3.31$	53	−5		−58	253
$a_{\beta_{CO}} = -1.05$, $a_{\beta_{FeC}} = 3.61$	117	−14		−131	28
fitted β_{CO}, β_{FeC}, k_{FeCO}					
$\beta_{CO} = 2.05$, $\beta_{FeC} = 3.18$, $k = 45.6$	43	−34	35	−77	50.6

[a] All values are reported in CHARMM AKMA units (energies in kcal mol^{-1}, distances in Å), except cooling time, T_1, which is reported in ps. $\delta\nu_{Fe-C}$ describes the shift in Fe−C_{CO} vibrational frequency of the simulated results from the experimental value (507 cm^{-1}). $\delta\nu_{CO}$ similarly describes the shift in CO vibrational frequency from 1949 cm^{-1}. $\delta\nu_{FeCO}$ reports the shift in the FeCO bending frequency from the experimental value of 570 cm^{-1}. $\delta(\nu_{CO}-\nu_{Fe-C})$ describes the difference in the separation of the CO and Fe−C_{CO} stretch frequencies between simulated and experimental values (1442 cm^{-1}). Effective models yield fast T_1 values at a minimum cost to the calculated vibrational spectra.

such as the heme doming motion were not found to significantly affect the cooling rate, although they may be important to dissipate energy away from the Fe−C_{CO} bond once it has been transferred. Energy transfer from CO to Fe−C_{CO} and the FeCO bending mode was identified as the rate determining step.

The effects of correlation of the Fe−C_{CO} and CO bond strengths, arising from back-bonding between the ligand and metal center, were examined within a classical MD framework. While coupled harmonic bonded potentials (model I) result in slightly more efficient ligand relaxation than those using fixed bond force constants, no great improvement leading to realistic CO cooling times was achieved without strongly affecting CO or Fe−C_{CO} vibrational frequencies. An analogous coupled anharmonic model was found to perform similarly to the noncoupled Morse model with fixed Morse parameters for both bonds.

The observables, relaxation time and infrared spectroscopy, were calculated within the framework of classical mechanics. Quantum corrections for both observables are available and have been investigated in the past. For the vibrational spectra, quantum corrections of the form $\propto \hbar\omega/(1 - \exp(-\hbar\omega/k_BT))$ primarily influence the band shape and maximum intensity[37] but not the position of the lines. For relaxation times, a recent study has established that nonequilibrium simulations for the $1 \rightarrow 0$ relaxation of the CO stretch lead to relaxation rates approximately 2−3 times longer than rates from quantum simulations.[46] Applying this correction to the classical rate $T_1 = 50$ ps calculated here gives a relaxation time of 17 to 25 ps which is in very good agreement with experiment. In

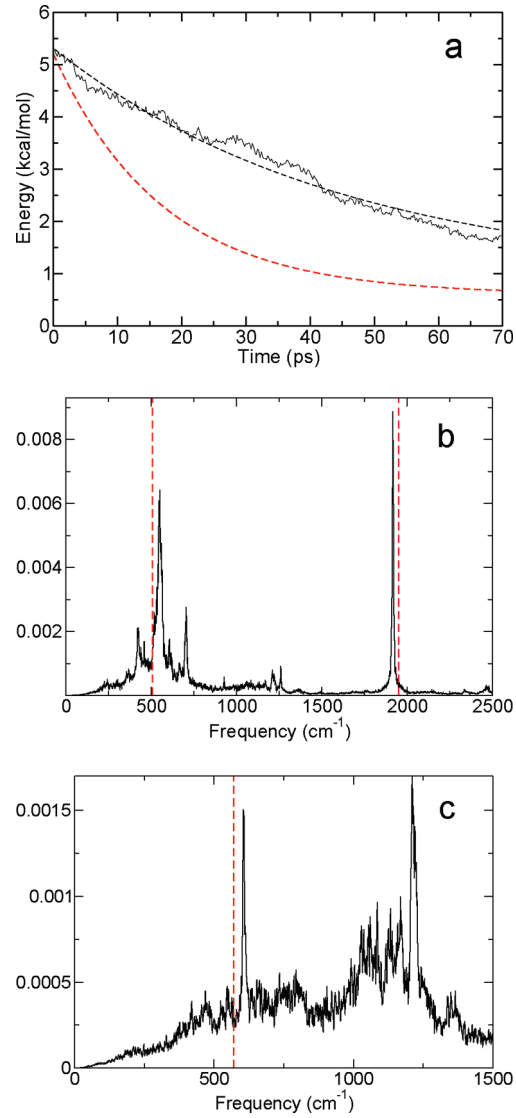

Figure 7. (a) CO relaxation curve. The black dashed line shows the fitted decay curve. An exponential decay curve with the experimental cooling constant $T_1 = 17$ ps is shown for reference as the red dashed line. (b) Fe−C_{CO} bond vibrational spectrum. The red dashed lines mark the positions of experimental spectral peaks. (c) Vibrational spectrum of the FeCO bending mode. The red line marks the position of the experimental FeCO bending peak. Fitted values from I-NoLLS were used for the CO and Fe−C_{CO} Morse β parameters and the FeCO bending force constant.

conclusion, while quantum effects do play some role, the center frequency for vibrational bands is unaffected and application of rigorously investigated correction factors leads to improvement between the calculated and experimental values for the observables considered here.

As mentioned above, CO vibrations were fitted to the A_1 substate in MbCO. The structural assignment of this, and the other two spectroscopically characterized states A_0 and A_3, has been the subject of some debate in the literature. A recent mixed QM/MM/MD study has assigned the A_0 and A_1 states to the open conformation of $His^{64}H^+$ and the closed conformation of the His_ϵ^{64} tautomer, respectively,[47] whereas structural details concerning A_3 remain elusive. For A_3, all previously suggested structural interpretations (two rotamers of the imidazole side chain of $His_\epsilon 64$,[48] cooperative motion between $His_\delta 64$ and nearby Arg45[49]) could be ruled out. However, by combining results from experiments and simulations, it was concluded that

A_3 is related to A_1 through a larger structural change.[47,50] Finally, the line shapes of the A_1 and A_3 substates have been fitted,[51] which was not attempted here. Previous work on photodissociated CO in Mb and CO in ices has shown that it is possible to also describe the line shape correctly but only with suitably detailed electrostatic interactions[28,52] which was not further pursued here.

In all cases, coupling between CO, Fe−C_{CO}, and the FeCO bending mode can be improved significantly by reducing the separation in vibrational frequencies between them. Parameter optimization including information from the MD simulations was used to find an improved set of parameters that yield a reasonable cooling rate at a minimal cost to the accuracy of the spectroscopy. The resulting model keeps all individual stretch frequencies within 45 cm^{-1} of experimental values while decreasing the CO relaxation time to $T_1 = 50$ ps (25 to 17 ps including quantum corrections), a large improvement from the 432 ps cooling time achieved with the CHARMM22 standard force field. Further decrease in cooling time to reach values closer to experiment might be achieved by a more complete treatment of delocalized heme normal modes, or perhaps by fitting of a more elaborate potential energy surface analogous to the coupled Morse potential model to add additional degrees of freedom.

Acknowledgment. The authors gratefully acknowledge financial support from the Swiss National Science Foundation under grant 200021-117810.

References and Notes

(1) Ota, N.; Agard, D. *J. Mol. Biol.* **2005**, *351*, 345.
(2) Sharp, K.; Skinner, J. J. *Proteins: Struct., Funct., Bioinf.* **2006**, *65*, 347.
(3) Whitnell, R. M.; Wilson, K. R.; Hynes, J. T. *J. Phys. Chem.* **1990**, *94*, 8625.
(4) Sagnella, D. E.; Straub, J. E. *Biophys. J.* **1999**, *77*, 70.
(5) Sagnella, D.; Straub, J. E. *J. Phys. Chem. B* **2001**, *105*, 7057.
(6) Bu, L.; Straub, J. *Biophys. J.* **2003**, *85*, 1429.
(7) Henry, E. R.; Eaton, W. A.; Hochstrasser, R. M. *Proc. Natl. Acad. Sci.* **1986**, *83*, 8982.
(8) Mizutani, Y.; Kitagawa, T. *Chem. Rec.* **2001**, *1*, 258.
(9) Danielsson, J.; Meuwly, M. *J. Phys. Chem. B* **2007**, *111*, 218.
(10) Montroll, E. W.; Shuler, K. E. *J. Chem. Phys.* **1957**, *26*, 454.
(11) Bethe, H. A.; Teller, E. Ballistic Research Laboratory, Report X-117 (1941).
(12) Shiga, M.; Okazaki, S. *J. Chem. Phys.* **1998**, *109*, 3542.
(13) Maradudin, A. A.; Fein, A. E. *Phys. Rev.* **1962**, *128*, 2589.
(14) Fujisaki, H.; Bu, L.; Straub, J. E. In *Normal Mode Analysis: Theory and Applications to Biological and Chemical Systems*; Cui, Q., Bahar, I., Eds.; Chapman and Hall/CRC Press: Boca Raton, FL, 2005; Chapter 15, pp 301−323.
(15) MacKerell, A. D., Jr.; Wiorkiewicz-Kurczera, J.; Karplus, M. *J. Am. Chem. Soc.* **1995**, *117*, 11946.
(16) Laage, D.; Demirdjian, H.; Hynes, J. T. *Chem. Phys. Lett.* **2005**, *405*, 453.
(17) Cupane, A.; Leone, M.; Unger, E.; Lemke, C.; Beck, M.; Dreybrodt, W.; Schweitzer-Stenner, R. *J. Phys. Chem. B* **1998**, *102*, 6612.
(18) Ladanyi, B. M.; Stratt, R. M. *J. Chem. Phys.* **1999**, *111*, 2008.
(19) Vogel, K. M.; Kozlowski, P. M.; Zgierski, M. K.; Spiro, T. G. *Inorg. Chim. Acta* **2000**, *297*, 11.
(20) Owrutsky, J. C.; Li, M.; Locke, B.; Hochstrasser, R. M. *J. Phys. Chem.* **1995**, *99*, 4842.
(21) Hill, J. R.; Tokmakoff, A.; Peterson, K. A.; Sauter, B.; Zimdars, D.; Dlott, D. D.; Fayer, M. D. *J. Phys. Chem.* **1994**, *98*, 11213.
(22) Leu, B. M.; Silvernail, N. J.; Zgierski, M. Z.; Wyllie, G. R.; Ellison, M. K.; Scheidt, W. R.; Zhao, J.; Sturhahn, W.; Alp, E. E.; Sage, J. T. *Biophys. J.* **2007**, *92*, 3764.
(23) Heilweil, E. J.; Cavanagh, R. R.; Stephenson, J. C. *Chem. Phys. Lett.* **1987**, *134*, 181.
(24) Ansari, A.; Berendzen, J.; Braunstein, D.; Cowen, B. R.; Frauenfelder, H.; Kyung Hong, M.; Iben, I. E. T.; Johnson, J. B.; Ormos, P.; Sauke, T. B.; et al. *Biophys. Chem.* **1987**, *26*, 337.
(25) Brooks, B. R.; Bruccoleri, R. E.; Olafson, B. D.; States, D. J.; Swaminathan, S.; Karplus, M. *J. Comput. Chem.* **1983**, *4*, 187.
(26) MacKerell, A. D., Jr.; Bashford, D.; Bellott, M.; Dunbrack, R. L., Jr.; Evanseck, J. D.; Field, M. J.; Fischer, S.; Gao, J.; Guo, H.; Ha, S.; et al. *J. Phys. Chem. B* **1998**, *102*, 3586.
(27) Kuriyan, J.; Wilz, S.; Karplus, M.; Petsko, G. A. *J. Mol. Biol.* **1986**, *192*, 133.
(28) Plattner, N.; Meuwly, M. *Biophys. J.* **2008**, *94*, 2505.
(29) Meuwly, M. *ChemPhysChem* **2006**, *10*, 2061.
(30) Nutt, D. R.; Meuwly, M. *Biophys. J.* **2003**, *85*, 3612.
(31) Nutt, D. R.; Meuwly, M. *Proc. Natl. Acad. Sci.* **2004**, *101*, 5998.
(32) Brooks, C. L.; Karplus, M. *J. Chem. Phys.* **1983**, *79*, 6312.
(33) Van Gunsteren, W. F.; Berendson, H. J. C. *Mol. Phys.* **1977**, *34*, 1311–1327.
(34) Meuwly, M.; Becker, O. M.; Stote, R.; Karplus, M. *Biophys. Chem.* **2002**, *89*, 183.
(35) McQuarrie, D. A. *Statistical Mechanics*; Harper's Chemistry Series: New York, 1976.
(36) Allen, M. P.; Tildesley, D. J. *Computer Simulation of Liquids*; Clarendon Press: Oxford, U.K., 1987.
(37) Schmitz, M.; Tavan, P. *J. Chem. Phys.* **2004**, *121*, 12247.
(38) Devereux, M.; Meuwly, M. (2009), in preparation.
(39) Law, M. M.; Hutson, J. M. *Comput. Phys. Commun.* **1997**, *102*, 252.
(40) Frisch, M. J.; Trucks, G. W.; Schlegel, H. B.; Scuseria, G. E.; Robb, M. A.; Cheeseman, J. R.; Montgomery, J. A., Jr.; Vreven, T.; Kudin, K. N.; et al. *Gaussian 03*, revision C.01; Gaussian, Inc.: Wallingford, CT, 2004.
(41) Becke, A. D. *J. Chem. Phys.* **1993**, *98*, 5648.
(42) Stephens, P. J.; Devlin, F. J.; Chabalowski, C. F.; Frisch, M. J. *J. Phys. Chem.* **1994**, *98*, 11623.
(43) Schäfer, A.; Horn, H.; Ahlrich, R. *J. Chem. Phys.* **1992**, *97*, 2571.
(44) Sagnella, D. E.; Straub, J. E.; Jackson, T. A.; Lim, M.; Anfinrud, P. A. *Proc. Natl. Acad. Sci.* **1999**, *96*, 14324–14329.
(45) Lumry, R.; Keyes, M. H.; Falley, M. *J. Am. Chem. Soc.* **1971**, *93*, 2035.
(46) Stock, G. *Phys. Rev. Lett.* **2009**, *102*, 118301.
(47) Devereux, M.; Meuwly, M. *Biophys. J.* **2009**, *96*, 4363.
(48) Merchant, K. A.; Noid, W. G.; Thompson, D. E.; Akiyama, R.; Loring, R. F.; Fayer, M. D. *J. Phys. Chem. B* **2003**, *107*, 4.
(49) Schulze, B.; Evanseck, J. D. *J. Am. Chem. Soc.* **1999**, *121*, 6444.
(50) Mueller, J. D.; McMahon, B. J.; Chien, E. Y. T.; Sligar, S. G.; Nienhaus, G. U. *Biophys. J.* **1999**, *77*, 1036.
(51) Mourant, J. R.; Braunstein, D. P.; Chu, K.; Frauenfelder, H.; Nienhaus, G. U.; Ormos, P.; Young, R. D. *Biophys. J.* **1993**, *65*, 1496.
(52) Plattner, N.; Meuwly, M. *ChemPhysChem* **2008**, *9*, 1271.

JP903741V